

# Supramolecular self-assembly formed from cucurbit[8]uril and *p*-hydroxybenzoic acid

Chenghui Wang,<sup>a</sup> Zhichao Yu,<sup>a</sup> Qing-hong Bai,<sup>a</sup> Dingwu Pan,<sup>a</sup> Timothy J. Prior,<sup>b</sup> Zhu Tao,<sup>a</sup> Carl Redshaw,<sup>b\*</sup> Xin Xiao,<sup>\*a</sup>

<sup>a</sup> Key Laboratory of Macrocyclic and Supramolecular Chemistry of Guizhou Province, Guizhou University, Guiyang 550025, China.

<sup>b</sup> Chemistry, School of Natural Sciences, University of Hull, Hull HU6 7RX, U.K.

E-mail: gyhxxiaoxin@163.com, xxiao@gzu.edu.cn (X. Xiao), C.Redshaw@hull.ac.uk (C. Redshaw)

## Abstract

The binding behavior of cucurbit[8]uril (Q[8]) and *p*-hydroxybenzoic acid (*p*-HBA) has been investigated using <sup>1</sup>H NMR titration experiments, UV/vis absorption, isothermal titration calorimetry (ITC), and X-ray crystallography. Results revealed that, in solution, the Q[8] can accommodate two *p*-HBA molecules to form a 1:2 host-guest inclusion complex, namely (*p*-HBA)<sub>2</sub>@Q[8]. From a poorly scattering crystal, we were able to identify two symmetry unique Q[8] rings, but with different *p*-HBA fillings. The structure can be represented as Q[8] + 1.5 *p*-HBA which gives Q[8]@(*p*-HBA)<sub>2</sub>.Q[8]@*p*-HBA as the structural formula. This supramolecular structure was screened for its ability to iodine capture. The experimental results showed that the adsorption efficiency of the supramolecular organic framework materials for iodine capture was 43.8%, with an equilibrium adsorption capacity of 223.3 mg/g.

## Introduction

Supramolecular chemistry is mainly concerned with the formation of complex but ordered molecular aggregates with definite microstructure and specific functions and formed through non-covalent bond interactions [1-4]. In supramolecular chemistry, host-guest recognition is at the core of supramolecular chemistry research. It refers to the process of a selected host combining with a particular guest and producing specific functions and is showing prospects for application in a variety of areas such as substance transport, energy transfer, electron transfer and functional materials [5-9]. As supramolecular chemistry has developed, new macrocyclic families have been discovered. One of the more recent additions to the field are the cucurbit[*n*]urils (Q[*n*]s or CB[*n*]s), a new type of synthetic receptor that can interact with a variety of organic compounds and ionic compounds. Their structure is characterized by a hydrophobic inner cavity and a hydrophilic port, and they possess strong structural rigidity. Q[*n*]s can selectively accommodate guest molecules of suitable size and shape, and thus exhibit extensive host-guest chemistry [12-16]. Electrostatic calculations have shown that the port of the cucurbit[*n*]uril is negative, and the outer surface is more positive, indicating that the outer surface of the cucurbit[*n*]uril is capable of interacting with anions and electron-rich substances, which would potentially provide sites for binding of iodide ions [17-18]. In the Q[*n*] family, the cucurbit[8]uril (Q[8] or CB[8]) has received much attention because of its has a large cavity (Figure 1a,b). For example, Yu, Liu and co-workers reported that the cucurbit[8]uril-based host-guest complex (Eu<sup>3+</sup>@PY-DPA-CB[8]) can tune full-color light-emitting materials. In addition, the host-guest complex can be used for multicolor imaging in cells [19]. Our research group has also reported a Q[8]-based porous supramolecular assembly (Q[8]-PSA) that can be used for drug adsorption and controlled release [20]. Such work suggests that cucurbit[8]uril has much potential for the preparation of supramolecular materials with useful applications.

*p*-Hydroxybenzoic acid (*p*-HBA) (Figure 1c), a monohydroxyphenolic acid, is a raw material that is utilized in organic synthesis and has a wide range of applications and usage [21-24]. Furthermore, *p*-HBA has been exploited for MOF construction, and resulting Ag-based MOFs were found to be efficient catalysts, in the presence of

sunlight, for the degradation of herbicides [25]. Lithium-based MOFs derived from *p*-HBA are also known [26].

In the work, the binding behaviour of the Q[8] and *p*-hydroxybenzoic acid (*p*-HBA) was investigated using  $^1\text{H}$  NMR titration experiments, UV/vis absorption, isothermal titration calorimetry (ITC), and X-ray crystallography. The results show that the Q[8] can accommodate two *p*-HBA molecules to form a 1:2 host-guest inclusion complex  $(p\text{-HBA})_2@Q[8]$  in solution, whilst in the solid state, the 1:1.5 inclusion complex  $Q[8]@(p\text{-HBA})_2 \cdot Q[8]@p\text{-HBA}$  was identified. We have previously reported the 3D framework  $\{\text{Cs}(\text{H}_2\text{O})[(p\text{-HBA})_2@Q[8]_2] \cdot 2p\text{-HBACl} \cdot 24\text{H}_2\text{O}\}$ , where the Cs is coordinated to the oxygens of the Q[8] portal, which is thought to be induced by the presence of the *p*-HBA [27]. We have investigated the potential application of  $Q[8]@(p\text{-HBA})_2 \cdot Q[8]@p\text{-HBA}$  for capture of iodine. The positive charge distribution on the outer surface of the cucurbit[8]uril is thought to be beneficial for such capture. The results show that the adsorption efficiency and capacity of the supramolecular framework material for iodine is 43.8% and 223.3 mg/g, respectively.

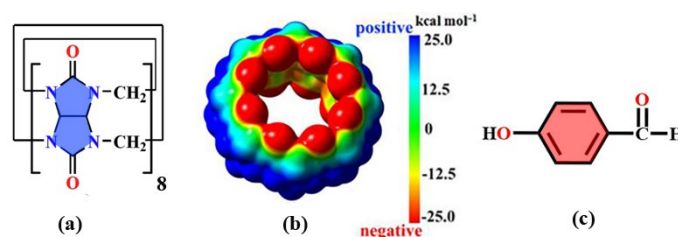


**Figure 1.** The structure of Q[8] and *p*-hydroxybenzoic acid.

## Results and discussion

The host-guest assembly of Q[8] and *p*-HBA were firstly investigated by  $^1\text{H}$  NMR spectroscopic titration experiments. As shown in the Figure 2, when adding 0.5 equiv. of Q[8] to *p*-HBA in  $\text{D}_2\text{O}$  (Figure 2b), the signals corresponding to Ha and Hb in the benzene ring exhibit upfield shifts from  $\delta$  7.67 to 7.66 ppm ( $\Delta\delta = 0.01$  ppm) and  $\delta$  6.69 to 6.66 ppm ( $\Delta\delta = 0.03$  ppm) compared to free *p*-HBA (Figure 2c). The result shows that benzene ring is included the cavity of the Q[8], and are shielded by the cavity of the Q[8].

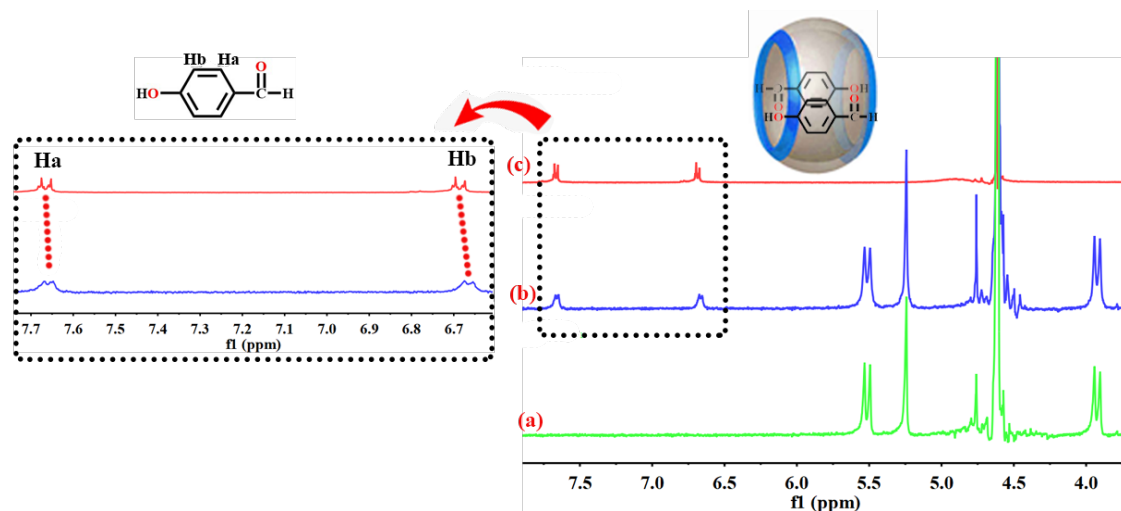


**Figure 2.**  $^1\text{H}$  NMR spectra obtained from the titration of *p*-HBA with Q[8]: (a) Neat Q[8]; (b) Q[8]: *p*-HBA = 1:2; (c) *p*-HBA.

To further study the interaction process between Q[8] and *p*-HBA, UV-vis titration experiments of Q[8]/*p*-HBA in the solution were performed. The free host Q[8] exhibits no absorbance at  $\lambda > 210$  nm. The UV-vis spectra obtained for the *p*-HBA aqueous solutions showed a strong absorption at 248 nm, attributed to the absorption peak of dissociated phenol hydroxyl group [28]. Upon addition of variable concentrations of Q[8] to the *p*-HBA aqueous solution, the absorption peak of the *p*-HBA gradually increased and red shifted to 253 nm, with a red shift of 5 nm (Figure 3a). This phenomenon indicates that the introduction of the Q[8] enhances the dissociation of the *p*-hydroxybenzoate. The ratio of absorbance (A) to mole number (N) of host Q[8] and *p*-HBA at 248 nm can be fitted with a 1:2 binding model (Figure 3b). Moreover, a continuous variation Job's plot (Figure 3c) further confirmed that the Q[8]/*p*-HBA host-guest complex is formed with a 1 : 2 stoichiometry.

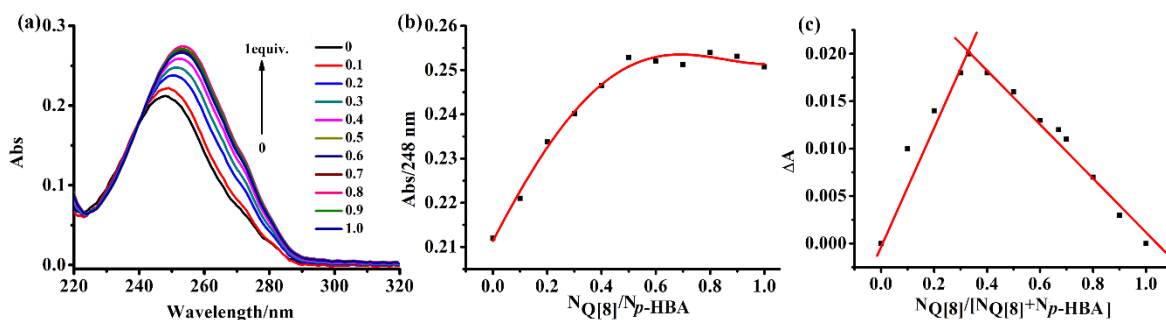


**Figure 3.** (a) The UV-vis titration of *p*-HBA ( $2 \times 10^{-5} \text{ mol}\cdot\text{L}^{-1}$ ) on increasing concentrations of Q[8]; (b) the concentrations and absorbance vs.  $N_{\text{Q}[8]}/N_{\text{p-HBA}}$  plots. (c) Continuous variation Job's plot for Q[8] and the guest on the basis of UV-vis titration spectra.

Next, isothermal titration calorimetry (ITC) was used to evaluate the host-guest interaction between Q[8] and *p*-HBA in aqueous solution (Figure S1, Table S1). The data for the ITC were performed using Nano ITC analyze software to give binding constant  $K_{a1} = 1.76 \times 10^5 \text{ M}^{-1}$  and  $K_{a2} = 4.94 \times 10^3 \text{ M}^{-1}$ , respectively, showing that strong supramolecular interactions Q[8]/*p*-HBA complex. The changes in enthalpy ( $\Delta H_1$  and  $\Delta H_2$ ) were  $-11.59 \text{ kJ}\cdot\text{mol}^{-1}$  and  $-5.51 \text{ kJ}\cdot\text{mol}^{-1}$ , respectively, showing that the formation of the Q[8]/*p*-HBA complex is a weakly exothermic process. The  $\Delta G$  ( $\Delta H - T\Delta S$ )  $< 0$ , indicating that the Q[8]/*p*-HBA complex formation is a spontaneous process. The thermodynamic parameters show that for Q[8] and *p*-HBA, the interaction process is enthalpy driven ( $|\Delta H| > T\Delta S$ ), and the associated enthalpy change mainly comes from the *p*-HBA and Q[8] port ion-dipole interactions and cavity hydrophobic effect.

Crystals of the inclusion compounds of Q[8] with *p*-HBA were readily obtained from solution, but none of the crystals was large. These crystals were inherently weakly diffracting and none of them gave wholly satisfactory scattering. We selected the best crystal and collected a full set of data, but this did not scatter appreciably beyond  $1.05 \text{ \AA}$ . However, it has been possible to use the data to solve and refine a structure that provides vital structural information and makes chemical sense. This process has allowed us to definitively identify the structure present and confirm the presence of an inclusion complex.

The unit cell obtained is a very large one ( $>17500 \text{ \AA}^3$ ) and contains Q[8], *p*-HBA, and

a huge volume of disordered water (corresponding to around 32 % of the crystal volume). The huge cell and presence of disordered water explain the poor scattering and very rapid drop off in scattering intensity.

The structure was solved using routine methods in SHELXT in the centric space group 15 in setting  $I2/a$ . The asymmetric unit contains two unique half Q[8] molecules and 1.5 molecules of *p*-HBA. The symmetry present generates complete Q[8] molecules and fills them with *p*-HBA but gives two different rings with two different fillings. The structure can be represented as Q[8] + 1.5 *p*-HBA which gives Q[8]@(*p*-HBA)<sub>2</sub>.Q[8]@*p*-HBA as the structural formula (Figure 4 and Figure S2).

The first symmetry-unique Q[8] (ring 1) is occupied by two *p*-HBA molecules in a centrosymmetric embrace such that the aromatic rings are staggered with respect to each other and their planes are separated by a distance of 3.364(16) Å. The two *p*-HBA molecules are arranged such that their planes subtend an angle of around 25 ° with the central plane of the Q[8] ring.

For the second symmetry-independent Q[8], the cavity is filled by two half-occupied *p*-HBA molecules. The most likely explanation is that each of these cavities is occupied at random by a molecule in one of the two possible positions. It is worth noting that the orientation of the *p*-HBA molecules differs from the ring 1; the angle subtended by the aromatic ring of the *p*-HBA to the central plane of the Q[8] is 87 °. In each ring there is a classical hydrogen bond from the phenol to one carbonyl of the Q[8]. The two different rings are shown in Figure 5.

This gives an overall stoichiometry of Q[8](*p*-HBA)<sub>1.5</sub> but there is water present that is not crystallographically resolved. This was modelled within Olex2 using a solvent mask. This gives an overall formula Q[8](*p*-HBA)<sub>1.5</sub>·3H<sub>2</sub>O. Although the data are modest (final R<sub>1</sub> = 0.1368) they provide very useful information about the stoichiometry of the complex and interesting insight into the orientation of the *p*-HBA within the Q[8] cavity.

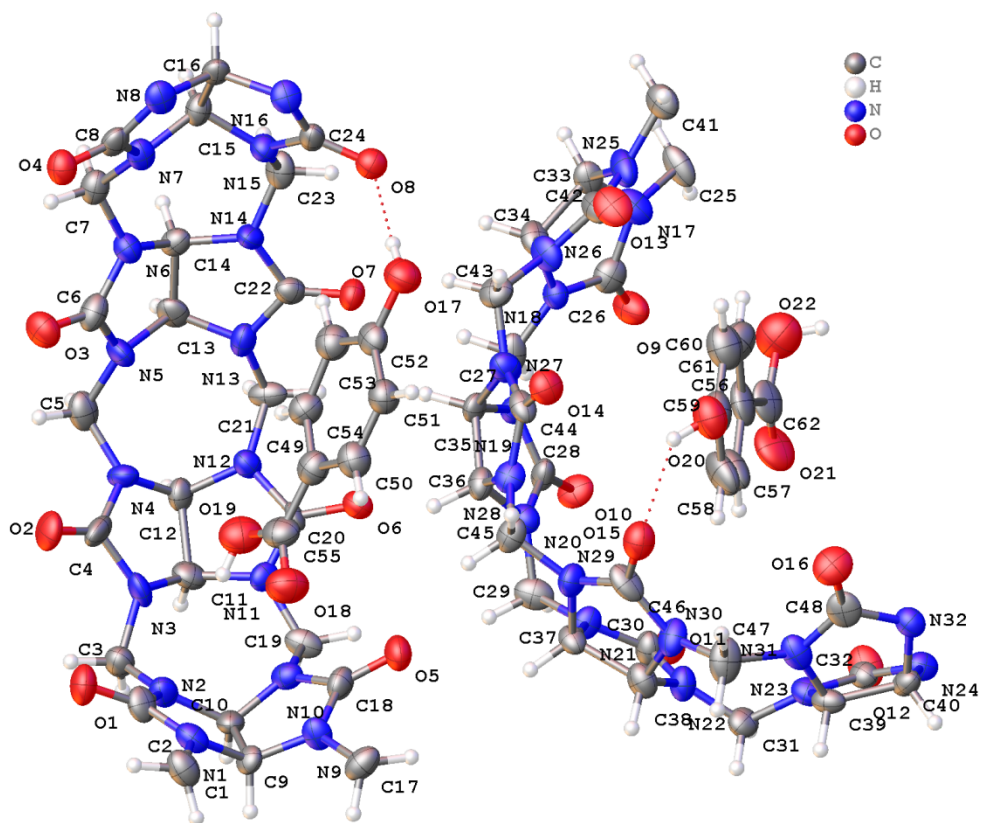


**Figure 4.** Asymmetric unit of  $Q[8](p\text{-HBA})_{1.5}\cdot 31\text{H}_2\text{O}$ . Atoms are drawn as 30 % probability ellipsoids. Dashed lines show the presence of hydrogen bonds. Disordered water is not illustrated.

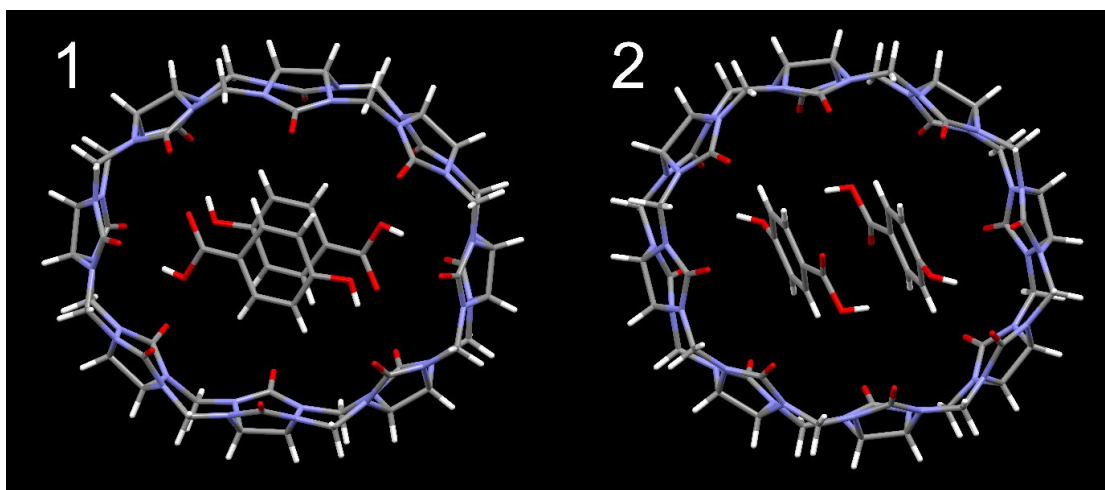


**Figure 5.** Two symmetry-unique filled  $Q[8]$  molecules. The guest  $p\text{-HBA}$  molecules in ring 1 are fully occupied. The guest  $p\text{-HBA}$  molecules in 2 are half occupied.

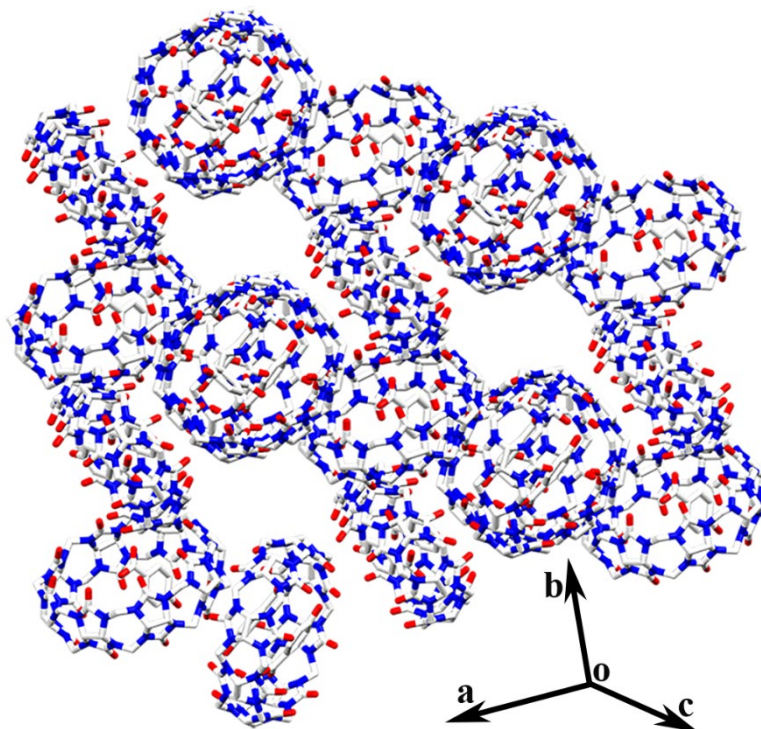


**Figure 6** Three-dimensional view of the crystal structure of Q[8]@(p-HBA)<sub>2</sub>.Q[8]@p-HBA.

**Table 1.** Crystal data and structure refinement for Q[8]@(p-HBA)<sub>2</sub>.Q[8]@p-HBA.

Empirical formula	C <sub>117</sub> H <sub>114</sub> N <sub>64</sub> O <sub>41</sub>
Formula weight	3072.72
Temperature/K	298
Crystal system	monoclinic
Space group	<i>I</i> 2/ <i>a</i>
<i>a</i> /Å	27.159(7)
<i>b</i> /Å	21.988(5)
<i>c</i> /Å	29.550(9)
$\alpha$ /°	90
$\beta$ /°	90.83(2)
$\gamma$ /°	90
Volume/Å <sup>3</sup>	17645(8)
<i>Z</i>	4
$\rho_{\text{calc}}$ g/cm <sup>3</sup>	1.157
$\mu$ /mm <sup>-1</sup>	0.091
F(000)	6368.0

Crystal size/mm <sup>3</sup>	0.21 × 0.18 × 0.15
Radiation	MoK $\alpha$ ( $\lambda = 0.71073 \text{ \AA}$ )
2 $\Theta$ range for data collection/ $^{\circ}$	4.532 to 39.562
Index ranges	$-37 \leq h \leq 37, -20 \leq k \leq 20, -25 \leq l \leq 25$
Reflections collected	166382
Independent reflections	7958 [Rint = 0.1608, Rsigma = 0.0509]
Data/restraints/parameters	7954/138/1046
Goodness-of-fit on F <sup>2</sup>	1.799
Final R indexes [ $I \geq 2\sigma(I)$ ]	R <sub>1</sub> = 0.1368, wR <sub>2</sub> = 0.3929
Final R indexes [all data]	R <sub>1</sub> = 0.1558, wR <sub>2</sub> = 0.4123
Largest diff. peak/hole / e $\text{\AA}^{-3}$	0.93/-0.56

Note that given that Q8 has a large cavity, it is able to encapsulate two *p*-HBA molecules in solution, thereby forming a 1:2 host guest inclusion complex. However, in the solid state, the Q[*n*]s portal carbonyl oxygen can interact with the positive electrostatic potential outer wall of adjacent Q[*n*]s through dipole interactions and hydrogen bonding interactions. These effects include the portal carbonyl oxygen atom of a Q[*n*] molecule with the methine unit of an adjacent Q[*n*], a bridging methylene unit, and dipole interactions or hydrogen bonding interactions between the portal carbonyl carbon atoms. These will shorten the distance between one Q[*n*] and the other adjacent Q[*n*], which may have a certain impact on the entry of some guest molecules into the cavity of the Q[*n*] during the crystallization process, resulting in the formation of a 1:1.5 inclusion complex in the crystalline state. As mentioned previously, we have previously reported a similar structure which has Cs present and different binding in the Q[8] but otherwise is surprisingly similar [27]. As can be seen from the three-dimensional view of the crystal structure (Figure 6), there is a certain channel structure between the cucurbit[8]urils. Given the outer surface of the cucurbit[8]uril is positively charged, and the iodine is an electron-rich substance, we speculate that the iodine can enter the channels between the cucurbit[8]uril, and use the outer surface interaction of the cucurbit[8]uril for iodine adsorption.

Iodine contamination is toxic and corrosive due to the ease of diffusion of iodine

vapor in the atmosphere, and is a great threat to the environment and human health [29,30]. To prevent this damage, the design of materials capable iodine capture has become an urgent research topic. We and others have previously employed Q[n]-based systems as well as other porous materials for I<sub>2</sub> capture [31-35].

Given the multiple noncovalent bonding interactions between Q[8] and *p*-HBA, Q[8]@(p-HBA)<sub>2</sub>.Q[8]@p-HBA and the channel structure formed between the cucurbit[8]tural, we envisaged that such a supramolecular organic framework material had potential for iodine capture. Prior to the experiment, we drew the standard curve of iodine solution by UV-vis absorption spectrum (Figure 7a, b), and used the standard curve to find the appropriate adsorption concentration of iodine solution. Next, 20 mg of Q[8]@(p-HBA)<sub>2</sub>.Q[8]@p-HBA was added to the fixed iodine-cyclohexane solution, and the absorption value of the solution was measured at different adsorption times (Figure 7c). With the extension of the adsorption process, the dark purple iodine solution faded significantly after 7 days in visible light (Figure 7d). In addition, the iodine adsorption efficiency of the Q[8]@(p-HBA)<sub>2</sub>.Q[8]@p-HBA in cyclohexane solution was evaluated to be 43.8 %, at an initial concentration of 4.0 × 10<sup>-4</sup> mol/L, and the equilibrium adsorption capacity of 223.3 mg/g. was obtained.

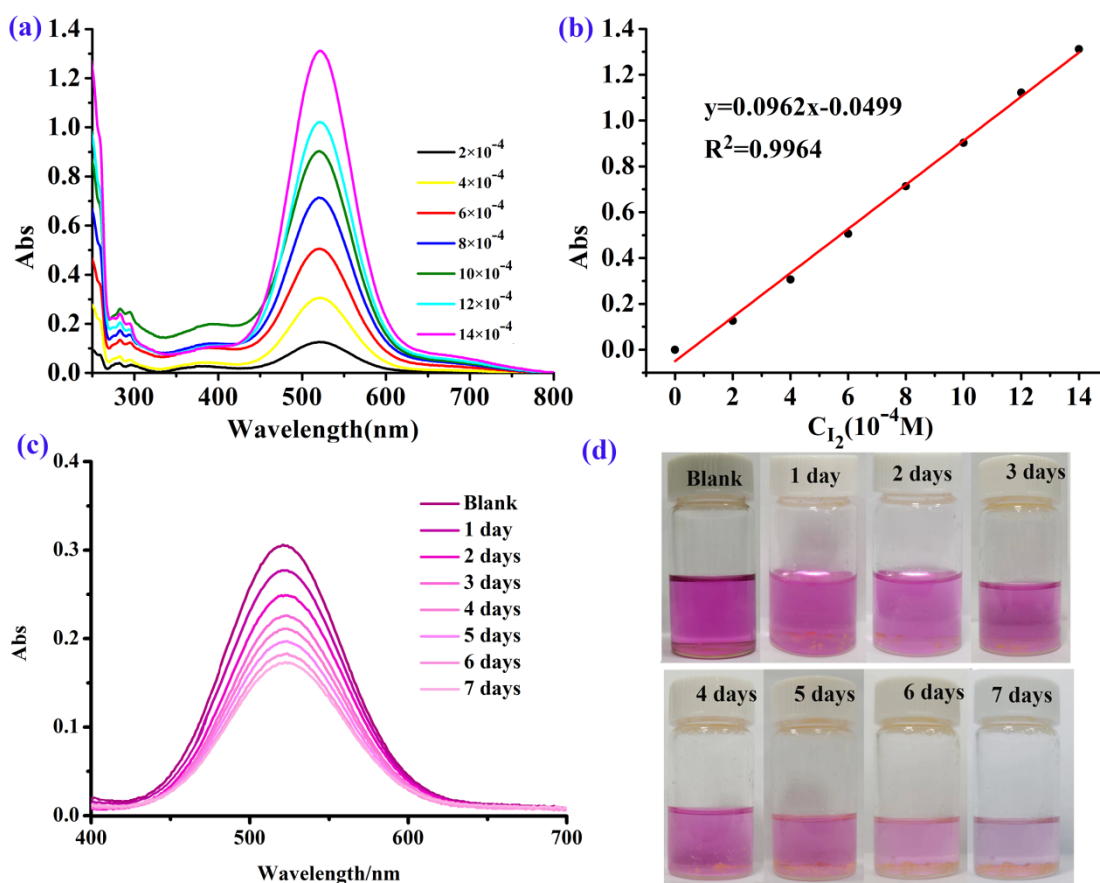


**Figure 7.** (a, b) UV absorption diagram and standard curve of  $I_2$  at different concentrations; (c) Time-dependent UV-vis spectra of cyclohexane solutions of iodine soaked in the  $Q[8]@(p\text{-HBA})_2.Q[8]@p\text{-HBA}$ ; (d) visual colour change of iodine cyclohexane solution after adding the crystal.

## Conclusion

In conclusion, a study of the interaction between cucurbit[8]uril (Q[8]) and *p*-hydroxybenzoic acid (*p*-HBA) reveals the formation of a 1:2 host-guest inclusion complex, namely  $(p\text{-HBA})_2@Q[8]$ . In the solid-state, using single crystal X-ray diffraction, we were able to identify a system with overall stoichiometry  $Q[8](p\text{-HBA})_{1.5} \cdot 3H_2O$ . The structural formula is  $Q[8]@(p\text{-HBA})_2.Q[8]@p\text{-HBA}$ , where one unique ring binds two *p*-HBA and the other only binds one, and the orientation of the guests is different. The  $Q[8]@(p\text{-HBA})_2.Q[8]@p\text{-HBA}$  could also capture iodine in cyclohexane solution with an appreciable adsorption efficiency of 43.3%, and the equilibrium adsorption capacity of 223.3 mg/g.

## Experimental section

### *Materials*

The guest *p*-hydroxybenzoic acid (*p*-HBA) was obtained from Aladdin (Shanghai, China). Q[8] was prepared and purified according to a literature method [36]. All other reagents were of analytical reagent grade and were used without any further purification. Deionized water was always used in the experiments.

### *<sup>1</sup>H NMR spectroscopy*

All the <sup>1</sup>H NMR spectra, including those for the titration experiments, were recorded at 298.15 K on a JEOL JNM-ECZ400S 400 MHz NMR spectrometer (JEOL) in D<sub>2</sub>O. D<sub>2</sub>O was used as a field-frequency lock and the observed chemical shifts are reported in parts per million (ppm) relative to that for the internal standard (TMS at 0.0 ppm).

In order to investigate the complexation of Q[8] with *p*-HBA in solution, <sup>1</sup>H NMR spectroscopic titration experiments were performed by adding increasing amounts of Q[8] to the solution of *p*-HBA in D<sub>2</sub>O.

### *UV-Vis absorption spectroscopy*

All UV-visible spectra were recorded from samples in 1 cm quartz cells on an UV-2700 spectrophotometer at room temperature. The Q[8] and *p*-HBA were dissolved in deionized water. The aqueous solution of *p*-HBA and Q[8] were prepared with a concentration of 1.0 mM and 0.1 mM, respectively. The UV-vis absorption experiments were performed by fixing the concentration of *p*-HBA at 20 μM and adding various amounts of Q[8] solution.

### *Isothermal titration calorimetry measurements.*

Thermodynamic parameters and binding constants (*K*<sub>a</sub>) for the host-guest complex were determined by titration calorimetry using a Nano ITC instrument (TA, USA). The

heat evolved was recorded at 298.15 K. Computer simulations (curve fitting) were performed using the Nano ITC analysis software. The concentration of Q[8] in the sample cell (1.3 mL) was  $1 \times 10^{-4}$  mol/L. The ITC titration was carried out by titrating the *p*-HBA solution ( $2 \times 10^{-3}$  mol/L, 10  $\mu$ L aliquots, at 250 s intervals) into a Q[8] solution.

#### *Single-crystal X-ray crystallography*

Single-crystal data for compound **1** were collected on the Bruker Smart Apex III CCD diffractometer with graphite monochromatic Mo- $K\alpha$  radiation ( $\lambda = 0.71073$  Å). Empirical absorption corrections were applied by using the multiscan program SADABS. Structural solution and full matrix least-squares refinement based on  $F^2$  were performed with the SHELXS-97 and SHELXL-97 program package, respectively [37]. Anisotropic thermal parameters were applied to all the non-hydrogen atoms. All hydrogen atoms were treated as riding atoms with an isotropic displacement parameter equal to 1.2 times that of the parent atom. The SQUEEZE routine of Platon was employed for all compounds because of the disordered solvent water molecules [38]. CCDC number 2226814 contains the supplementary crystallographic data for this paper.

#### *Preparation of complex Q[8]@(p-HBA)<sub>2</sub>.Q[8]@p-HBA*

Q[8] (5.0 mg, 0.0037 mmol) was added to a solution of *p*-HBA (10.0 mg, 0.072 mmol) in 6 mol/L HCl solution (3 mL). The mixture was heated until complete dissolution. Slow evaporation of the volatiles from the solution over a period of about two weeks, afforded block colorless crystals of complex Q[8]@(p-HBA)<sub>2</sub>.Q[8]@p-HBA.

#### *Iodine adsorption efficiency and capacity*

The iodine adsorption efficiency of the Q[8]@(p-HBA)<sub>2</sub>.Q[8]@p-HBA in organic solution was evaluated by formula [31]

$$\% \text{Pollutant removal efficiency} = \frac{C_0 - C_t}{C_0} \times 100\%$$

$C_0$  : the initial concentration of iodine;  $C_t$  : The concentration of solution at time  $t$  after adsorption

The equilibrium adsorption capacity is calculated by the following formula [32]

$$Q_t = \frac{(C_0 - C_t)V}{m}$$

$C_0$  (mg/L) : the initial concentrations of the iodine solution;  $C_t$  (mg/L) : the equilibrium concentrations of the iodine solution;  $m$  (g) is the weight of Q[8]@(*p*-HBA)<sub>2</sub>.Q[8]@*p*-HBA crystals used.

### Acknowledgments

This work was financially supported by the Science and Technology Fund of Guizhou Province. CR thanks the EPSRC for the award of an Overseas Travel Grant (EP/R023816/1).

### References

- [1] J. W. Steed and J. L. Atwood, *John Wiley and Sons*, 2022, **1**, 261-273.
- [2] J. M. Lehn, *Angew. Chem. Int. Ed. Eng.*, 1988, **27**, 89-112.
- [3] N. Lanigan and Wang, X, *Chem. Commun.*, 2013, **49**, 8133-8144.
- [4] C. Gao, Q. Wang, J. Li, C. H. Kwong, J. Wei, B. Xie, S. Lu, S. M. Y. Lee and R. Wang, *Sci. Adv.*, 2022, **8**, eabn1805
- [5] S. Guo, Q. Huang, Y. Chen, J. Wei, J. Zheng, L. Wang, Y. Wang and R. Wang, *Angew. Chem. Int. Ed.*, 2021, **60**, 618-623.
- [6] C. A. Schalley, *Int. J. Mass Spectrom.*, 2000, **194**, 11-39.
- [7] H. Yang, B. Yuan, X. Zhang and O. A. Scherman, *Acc. Chem. Res.*, 2014, **47**, 2106-2115.
- [8] S. B. Khan and S. L. Lee, *Molecules*, 2021, **26**, 3995.
- [9] X. Ji, F. Wang, X. Yan, S. Dong and F. Huang, *Chinese J. Chem.*, 2020, **38**, 1473-1479.
- [10] C. Sun, Z. Wang, L. Yue, Q. Huang, Q. Cheng and R. Wang, *J. Am. Chem. Soc.*, 2020, **142**, 16523-16527.

- [11] Z. Wang, C. Sun, K. Yang, X. Chen and R. Wang, *Angew. Chem*, 2022, **134**, e202206763; *Angew. Chemie Int. Ed.*, 2022, **61**, e202206763.
- [12] Y. Lu, Z. Yu, X. Yang, J. Dai, P. Shan, X. Feng, Z. Tao, C. Redshaw and X. Xiao, *Chin. Chem. Lett.*, 2022, 108040.
- [13] Y. Luo, W. Zhang, J. Zhao, M.-X. Yang, Q. Ren, C. Redshaw, Z. Tao and X. Xiao *Chin. Chem. Lett.*, 2022, 107780.
- [14] Y. Luo, W. Zhang, X. N. Yang, M. X. Yang, W. Min, Z. Tao and X. Xiao, *Inorg. Chem.* 2022, **61**, 16678-16684.
- [15] M. Liu, R. Cen, J. Li, Q. Li, Z. Tao, X. Xiao and L. Isaacs, *Angew. Chemie Int. Ed.*, 2022, **61**, e 202207209.
- [16] W. Zhang, Y. Luo, J. Zhao, C. Zhang, X. Ni, Z. Tao and X. Xiao, *Chinese Chem. Lett.*, 2022, **33**, 2455 – 2458.
- [17] X. D. Zhang, Y. Zhao, K. Chen, X. Y. Dao, Y. S. Kang, Y. Liu and W. Y. Sun, *Chem. Eur. J.*, 2020, **26**, 2154-2158.
- [18] J. X. Lin, J. Liang, J. F. Feng, B. Karadeniz, J. Lü and R. Cao, *Inorg. Chem. Front.*, 2016, **3**, 1393-1397.
- [19] H. J. Yu, X. L. Zhou, X. Dai, F. F. Shen, Q. Zhou, Y. M. Zhang, X. F. Xu and Y. Liu, *Chem. Sci.*, 2022, **13**, 8187-8192.
- [20] H. Feng, Y. Luo, M. Liu, Q. Chen, Z. Tao and X. Xiao, *New J. Chem.*, 2021, **45**, 22133-22140.
- [21] F. J. Rivas, F. J. Beltrán, J. Frades and P. Buxeda, *Water Research*, 2001, **35**, 387-396.
- [22] M. G. Soni, I. G. Carabin and G. A. Burdock, *Food Chem. Toxicol.*, 2005, **43**, 985-1015.
- [23] J. Yang, B. Hong, N. Wang, X. Li, X. Huang, Y. Bao, C. Xie and H. Hao, *CrystEngComm*, 2019, **21**, 6374-6381.
- [24] M. Lever, *Biochem. Med.*, 1973, **7**, 274-281.
- [25] P. Hayati, Z. Mehrabadi, M. Karimi, J. Janczak, K. Mohammadi, G. Mahmoudi, F. Dadi, M. J. S. Fard, A. Hasanzadeh and S. Rostamnia, *New J. Chem.*, 2021, **45**, 3408-3417.

- [26] X. Zhao, M. S. Shimazu, X. Chen, X. Bu and P. Feng, *Angew Chemie. Int. Ed.* 2018, **57**, 6208-6211.
- [27] K. Chen, L.-L. Liang, H. Cong, X. Xiao, Y.-Q. Zhang, S.-F. Xue, Q.-J. Zhu and Z. Tao, *CrystEngComm*. 2012, **4**, 3862-3864.
- [28] E. E. Sager, M. R. Schooley, A. S. Carr and S. F. Acree, *J. Res. Nat. Bur. Stand.*, 1945, **35**, 521-538
- [29] R. Chen, T. Hu and Y. Li, *React. Funct. Polym.*, 2020, **159**, 104806.
- [30] T. C. Chang, Y. H. Liu, M. L. Chen, C. C. Tseng, Y. S. Lin and S. L. Huang, *Molecules*, 2021, **26**, 3443.
- [31] J.H. Hu, R. Cen, M. Liu, P.-H. Shan, T. J. Prior, C. Redshaw, Y. Huang, Z. Tao and X. Xiao, *Inorg. Chem. Comm.* 2022, **142**, 109663.
- [32] X.D. Zhang, Y. Zhao, K. Chen, X.Y. Dao, Y.S. Kang, Y. Liu and W. Y. Sun, *Chem. Eur. J.* 2020, **26**, 2154-2158.
- [33] K. R. K. K. Reddy, T. S. Cavallini, G. J. F. Demets and L. F. Silva Jr, *New J. Chem.* 2014, **38**, 2262-2264.
- [34] A. Meng, J. Xing, Z.J. Li and Q.D. Li, *ACS Appl. Mater. Interfaces* 2015, **7**, 27449–27457.
- [35] R. Gong, J.J. Ye, W. Dai, X.Y. Yan, J. Hu, X. Hu, S. Li and H. Huang, *Ind. Eng. Chem. Res.* 2013, **52**, 14297–14303.
- [36] J. Lagona, P. Mukhopadhyay, S. Chakrabarti and L. Isaacs L, *Angew. Chem. Int. Ed.*, 2005, **44**, 4844-4870.
- [37] G. M. Sheldrick, *Acta Crystallogr. Sect. A.* 2008, **64**, 112-122.
- [38] A. L. Spek, *Acta Crystallogr. Sect. D.* 2009, **65**, 148-155.